Supplemental Materials

Table 1. List of antibodies used

Antibody (species-antigen)	Use	Dilution	Source	Ref.
Rabbit-CUL3*	WB	1:2000	Bethyl Laboratories A301-109A	(1)
Rabbit-CUL3*	IF	1:100	Bethyl Laboratories A301-109A	(1)
Rabbit-pNCC (T53)*	WB	1:2000	Ellison Lab	(2-4)
Rabbit-pNCC (T53)*	IF	1:10000	Ellison Lab	(4)
Rabbit-tNCC*	WB	1:6000	Ellison Lab	(2-4)
Rabbit-tNCC*	IF	1:8000	Ellison Lab	(3, 4)
Rabbit-pNKCC2 (T96/T101)	WB	1:1500	Bachmann Lab	(2-4)
Rabbit-pNKCC2 (T96/T101)	IF	1:8000	Bachmann Lab	(2-4)
Guinea pig-tNKCC2	WB	1:1500	Bachmann Lab	(2, 3)
Guinea pig-tNKCC2	IF	1:4000	Bachmann Lab	(3, 4)
Rabbit-N-WNK4*	WB	1:1000	Ellison Lab	(3, 5)
Rabbit-N-WNK4*	IF	1:4000	Ellison Lab	(3, 5)
Rabbit-C-SPAK*	IF	1:5000	McCormick Lab	(4)
Guinea pig-Parvalbumin	IF	1:2000	Swant, GP72	
Mouse-Calbindin	IF	1:2000	Swant, Calbindin D-28, (mouse 300)	
Rabbit-KLHL2/3	WB	1:1000	Santa Cruz Biotechnology	(3)
Rabbit-OSR1*	IF	1:4000	Delpire Lab	(2)
Sheep-C-WNK1	IF	1:200	MRC-PPU S062B	(6)
Rabbit-Nedd8	WB	1:1000	Cell Signaling (19E3)	
Rabbit-KLHL3*	IF	1:250	Proteintech 16951	

*CUL3, KLHL3, NCC, pNCC, WNK4, SPAK, and OSR1 antibodies have been validated in knockout mice.

Supplemental Figure Legends

Supplemental Figure 1. Normalization of Western blot data by Coomassie gel, compared with actin normalization.

To avoid normalization to actin, which can change abundance in response to experimental manipulation, and reaches saturating levels when as little as 3 µg is loaded per lane (7) we used the method recommended by McDonough and colleagues (7). A) An example is given for phosphorylated Na^+-Cl^- cotransporter (NCC) (pNCC), but the same approach was used for all blots presented. 20 µg (as determined by DC protein assay (Biorad, Inc)) of each sample was resolved on a gel, followed by staining with G-250 Coomassie (Bio-Rad, Inc). The stained gel was scanned, and five bands were selected (mainly of a molecular weights similar to that of pNCC) for densitometric quantification using ImageJ. Values were normalized to the mean density for that band in all eight samples, defined as 1.0. For pNCC Western blotting, gel loading volumes were then adjusted based on this analysis. The membrane was cut, and blotted for pNCC or β-actin. pNCC abundance was normalized to either β-actin or Coomassie (see graphs on right). In this example, variability between the actin and Coomassie approaches was similar, as was the fold-difference in pNCC between control and CUL3-Het/Δ9 mice. B) Following the same procedure pNCC abundance was determined in control and CUL3-Het mice, both actin and Coomassie approaches revealed no significant difference in pNCC abundance between the two strains.

Supplemental Figure 2. Electrophoretic migration of neddylated species is altered in CUL3-Het/Δ9 mice.

Neural precursor cell expressed developmentally down-regulated protein 8 (Nedd8) is a 9KDa protein that is covalently attached to Cullins. Western blotting for Nedd8 revealed that there were no differences in abundance of Nedd8-conjugated proteins (Nedd8-Cullins, which run at about 75KDa) between controls and CUL3-Het or CUL3-Het/Δ9. However, the signal obtained from kidney lysates of CUL3-Het/Δ9 mice appeared qualitatively different to those in CUL3-Het lysates, and may represent neddylated CUL3-Δ9 since it runs lower than the band in control. An actin blot performed on the same membrane is shown to support this (actin signal is running almost straight). For quantification (graphs below blots), band depth was measured using ImageJ by selecting bands and measuring the length (in arbitrary units) of the base of the histogram generated. Quantification revealed band depth was significantly greater in CUL3-Het/Δ9 lysates, suggests increased abundance of Nedd8-conjugated species. Mean values ± SEM, values in parentheses = n. CUL3-Het versus control, p=0.94; CUL3-Het/Δ9 versus control, *p =0.009, unpaired T-tests.

Supplemental Figure 3. Immunofluorescence for phosphorylated Na^+-Cl^- cotransporter (pNCC) corroborates Western blot (WB) data.

A) Signal for pNCC (green) was more intense in CUL3-Het/Δ9 mice than in control or in CUL3-Het mice, consistent with the data obtained by WB (Figs 2A and B). DAPI (blue) stains nuclei. Representatives of 4 independent experiments. White scale bars = 100 microns.

Supplemental Figure 4. Direct comparison of CUL3-Het and CUL3-Het/Δ9 mice confirms increased abundances of total and phosphorylated Na^+-Cl^- cotransporter (NCC).

Western blotting of whole kidney lysate confirmed that compared with CUL3-Het mice, CUL3-Het/Δ9 mice displayed increased abundances of NCC phosphorylated at threonine 53 (pNCC, *p=0.01), and total NCC (tNCC, *p=0.01) and pNCC/tNCC (*p=0.0009).

Supplemental Figure 5. Systolic blood pressure (SBP) is higher in CUL3-Het/Δ9 mice than in control mice.

Radiotelemetric blood pressure measurement revealed higher SBP in CUL3-Het/Δ9 compared with both control and CUL3-Het mice on a normal (0.49% NaCl) diet. Mean of the hourly averages over three dark periods are shown ± SEM, values in parentheses = n. CUL3-Het/Δ9 versus control or CUL3-Het mice, *p <0.0001, Post-hoc one-way analysis of variance (ANOVA): Tukey's multiple comparisons test. Blood pressure did not differ significantly between control and CUL3-Het mice.

Supplemental Figure 6. Exclusively apical localization of With-No-Lysine [K] Kinase 4 (WNK4), STE20 (Sterile 20)/SPS-1 related proline/alanine-rich kinase (SPAK), and Oxidative stress-response kinase-1 (OSR1) in medulla of CUL3-Het/Δ9 mice.

Signal for WNK4 in the medulla was more intense in CUL3-Het/Δ9 mice than in control or in CUL3-Het mice, consistent with the data obtained by Western blot for whole kidney lysate, Figs 2C and 2D), but in contrast to its distribution in some cortical segments, was not punctate.

Immunofluorescence for SPAK and OSR1 revealed exclusively apical localization in the medulla in both CUL3-Het and CUL3-Het/Δ9 mice. Representatives of 8 independent experiments. White scale bar = 100 microns.

Supplemental Figure 7. Oxidative stress-response kinase-1 (OSR1), like STE20 (Sterile 20)/SPS-1 related proline/alanine-rich kinase (SPAK), shows a strong punctate localization in CUL3-Het/Δ9 mice, but only in Na^+-K^+-$2Cl^-$ cotransporter (NKCC2)-negative segments.

A) Shows images at standard brightness, and B) with the brightness increased 3x, since OSR1 signal in CUL3-Het mice was not visible in A), but when made visible in B), the signal in CUL3-Het/Δ9 mice was oversaturated. For clarity, both are shown. In CUL3-Het mice, OSR1 (green) was distributed at the apical membrane in small cytoplasmic puncta in Parvalbumin-positive (red) Distal Convoluted Tubule 1 (DCT1), but only at the apical membrane in NKCC2-positive (red) cortical Thick Ascending Limb (TAL). In CUL3-Het/Δ9 mice, OSR1 signal was strongly localized to large puncta, along DCT1, and also along some Parvalbumin-negative segments (probably DCT2 and Connecting Tubule (CNT) and/or Cortical Collecting Duct (CCD) (CNT/CCD)). Representatives of 2 independent experiments. In A and B, white scale bars = 50 microns.

Supplemental Figure 8. With-No-Lysine [K] Kinase 1 (WNK1) abundance is greater and it localizes to large puncta along the Distal Convoluted Tubule (DCT) in CUL3-Het/Δ9 mice.

Immunofluorescence for WNK1 showed low abundance in small intracellular puncta in control and CUL3-Het mice, along Na^+-Cl^- cotransporter (NCC)-positive segments (DCT). In CUL3-Het/Δ9 mice, WNK1 abundance was much greater, and it was located in large puncta. Representatives of 2 independent experiments. White scale bars = 50 microns.

Supplemental Figure 9. Quantification of STE20 (Sterile 20)/SPS-1 related proline/alanine-rich kinase (SPAK) puncta reveals that they are of similar abundance, but larger in size, in CUL3-Het/Δ9 mice.

A) Confocal images of SPAK distribution from control, CUL3-Het and CUL3-Het/Δ9 mice, with examples of puncta of different areas circled, including 0.6 μm^2, which was selected as the cutoff size for "large" puncta. Redistribution of SPAK to larger intracellular puncta was observed in at least eight CUL3-Het/Δ9 mice, and a representative animal from each group was selected for analysis. 15-19 tubules of similar size were identified for each group (average tubule cross-sectional area: Control, 859 μm^2; CUL3-Het, 978 μm^2; CUL3-Het/Δ9, 939 μm^2) and analyzed using the ImageJ particle analysis tool. The number and intensity of fluorescent points within outlined tubules was counted. B) The average number of puncta was calculated per area of tubule, and did not differ between groups. C) The average size of puncta did not differ between Control and CUL3-Het mice, but was significantly greater in CUL3-Het/Δ9 mice. In B) to D) mean values are shown ± SEM, values in parentheses = n. CUL3-

Het/Δ9 versus control or CUL3-Het mice, *p <0.0001, Post-hoc one-way analysis of variance (ANOVA): Tukey's multiple comparisons test.

Supplemental Figure 10. Abundances of Kelch-like 2/3 (KLHL2/3) are not reduced in CUL3-Het/Δ9 mice.

Western blotting of whole kidney lysate using a commercial antibody that recognizes both KLHL2 and KLHL3 did not reveal differences in their abundances between A) Control and CUL3-Het mice or B) Control and CUL3-Het/Δ9 mice. For quantification, densitometric values were normalized using Coomassie stained gels (see Supplemental Fig 1 for details) and plotted as means ± SEM; values in parentheses = *n*.

Supplemental Figure 11. Kelch-like 3 (KLHL3) abundance and localization do not appear altered in CUL3-Het/Δ9 mice.

Immunofluorescence was performed using an antibody against KLHL3 that has been validated in KLHL3 KO mice. A) In control (equivalent to wild type) mice, consistent with our previous findings (3), KLHL3 localized to the cytoplasm along the distal convoluted tubule as shown by co-localization with parvalbumin (PV) and calbindin (CB, which is also a marker for connecting tubule). Abundance and localization of KLHL3 appeared similar in B) CUL3-Het mice and C) CUL3-Het/Δ9 mice. Representatives of 8 independent experiments. White scale bar = 50 microns.

Supplemental References

1. Agbor LN, Ibeawuchi SC, Hu C, Wu J, Davis DR, Keen HL, et al. Cullin-3 mutation causes arterial stiffness and hypertension through a vascular smooth muscle mechanism. *JCI Insight.* 2016;1(19):e91015.
2. Ferdaus MZ, Barber KW, Lopez-Cayuqueo KI, Terker AS, Argaiz ER, Gassaway BM, et al. SPAK and OSR1 play essential roles in potassium homeostasis through actions on the distal convoluted tubule. *The Journal of physiology.* 2016;594(17):4945-66.
3. McCormick JA, Yang CL, Zhang C, Davidge B, Blankenstein KI, Terker AS, et al. Hyperkalemic hypertension-associated cullin 3 promotes WNK signaling by degrading KLHL3. *The Journal of clinical investigation.* 2014;124(11):4723-36.
4. McCormick JA, Mutig K, Nelson JH, Saritas T, Hoorn EJ, Yang CL, et al. A SPAK isoform switch modulates renal salt transport and blood pressure. *Cell metabolism.* 2011;14(3):352-64.
5. Terker AS, Zhang C, McCormick JA, Lazelle RA, Zhang C, Meermeier NP, et al. Potassium modulates electrolyte balance and blood pressure through effects on distal cell voltage and chloride. *Cell metabolism.* 2015;21(1):39-50.
6. Schumacher FR, Siew K, Zhang J, Johnson C, Wood N, Cleary SE, et al. Characterisation of the Cullin-3 mutation that causes a severe form of familial hypertension and hyperkalaemia. *EMBO Mol Med.* 2015;7(10):1285-306.
7. McDonough AA, Veiras LC, Minas JN, and Ralph DL. Considerations when quantitating protein abundance by immunoblot. *Am J Physiol Cell Physiol.* 2015;308(6):C426-33.

Supplementary Figure 1.

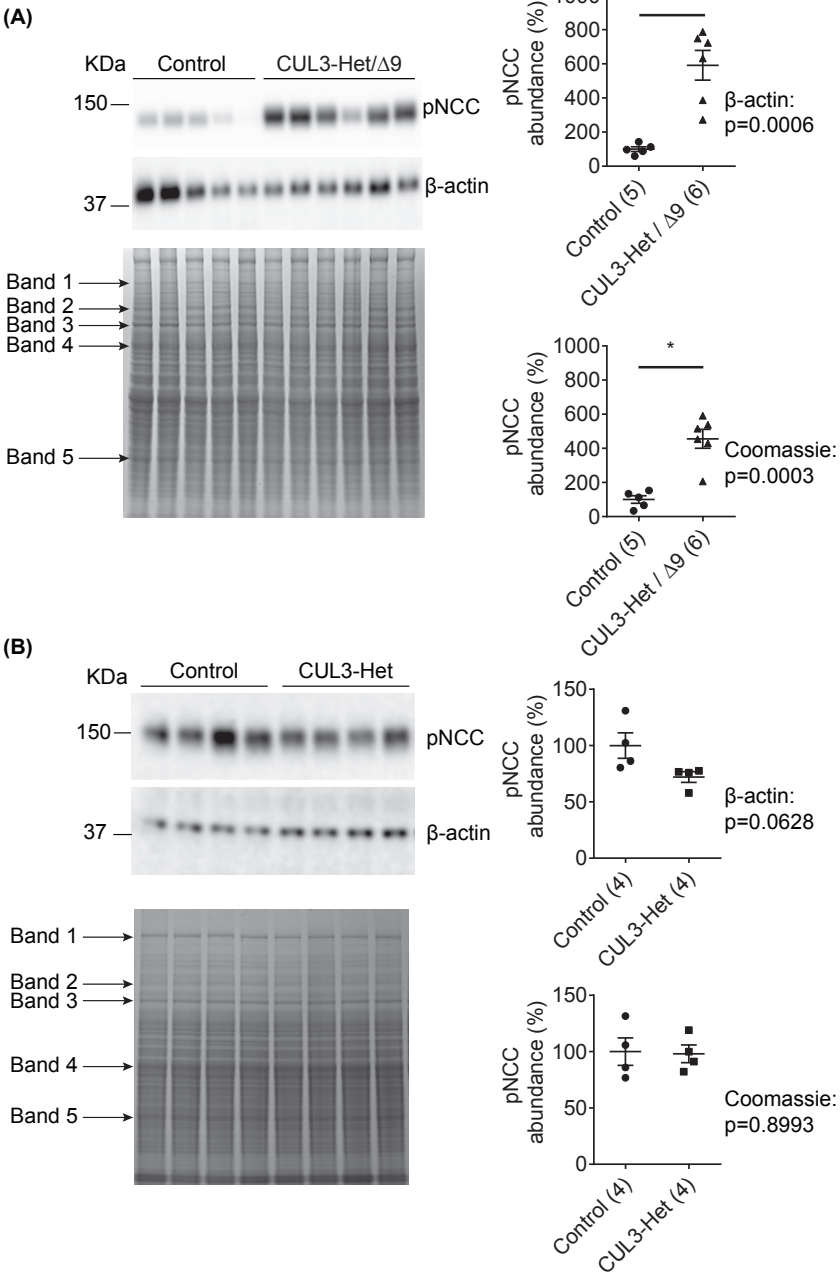

Supplementary Figure 2.

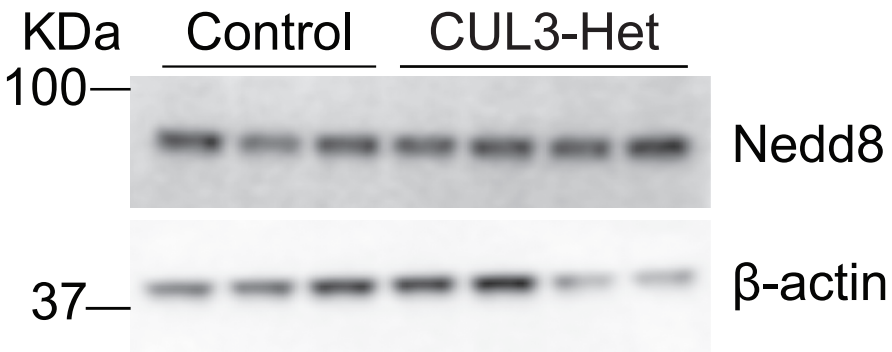

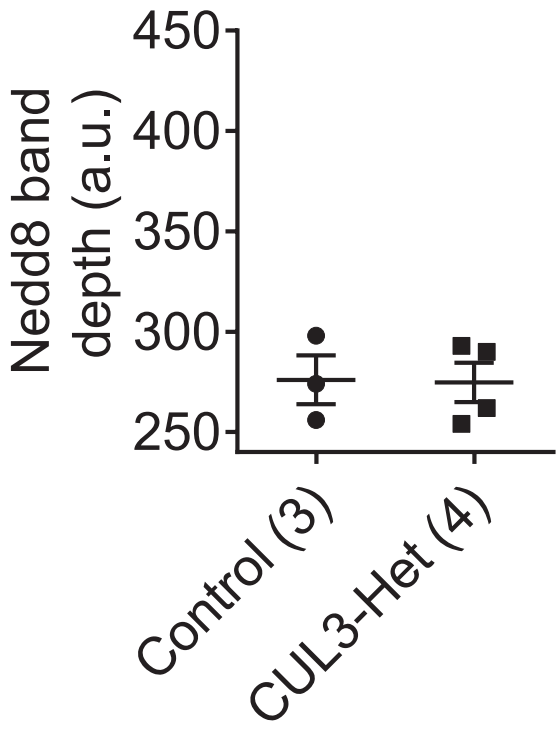

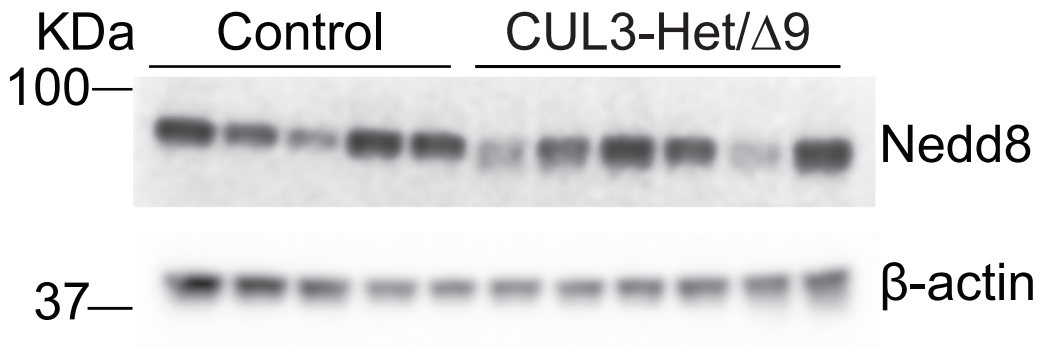

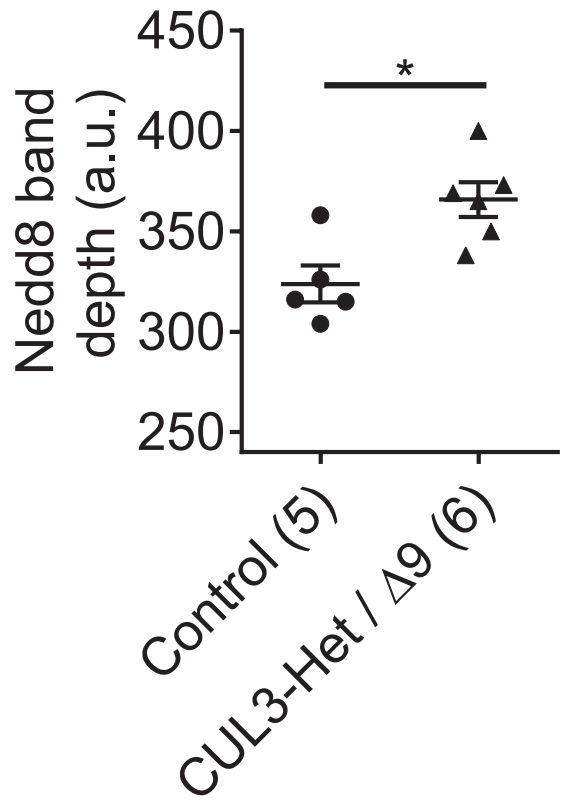

Supplementary Figure 3.

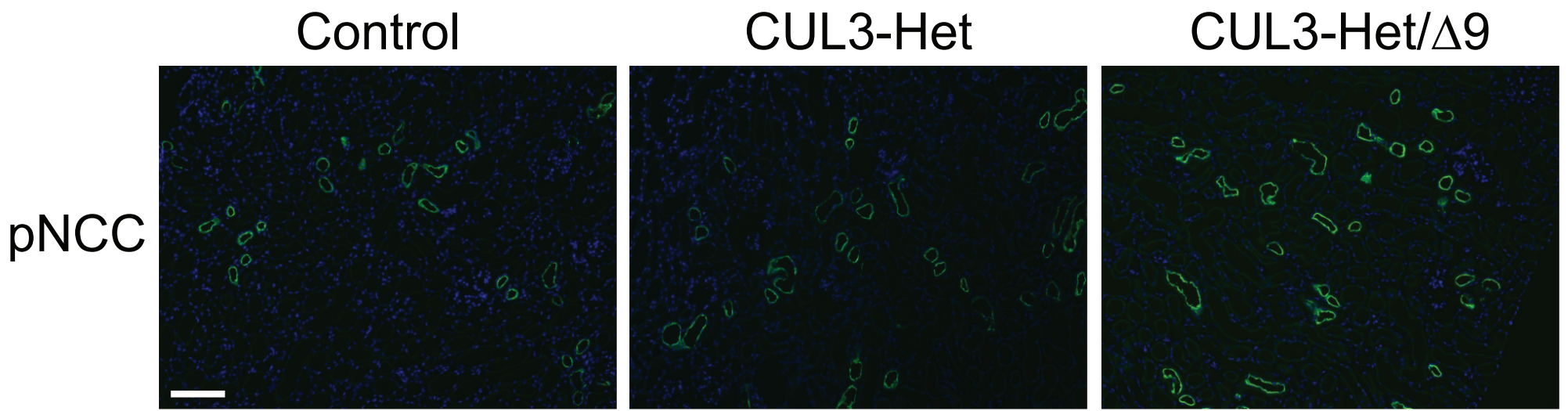

Supplementary Figure 4.

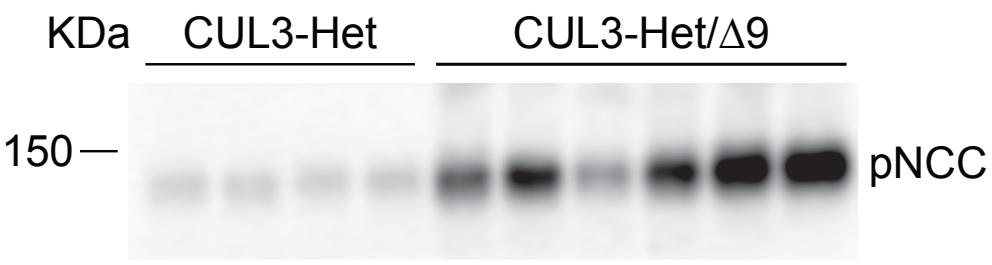

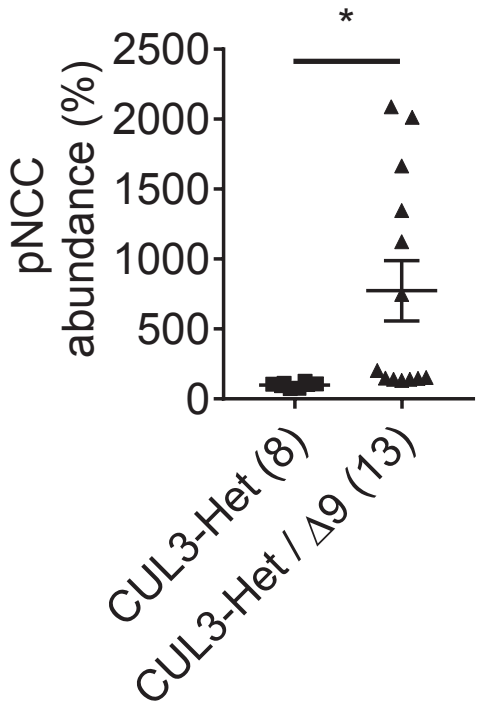

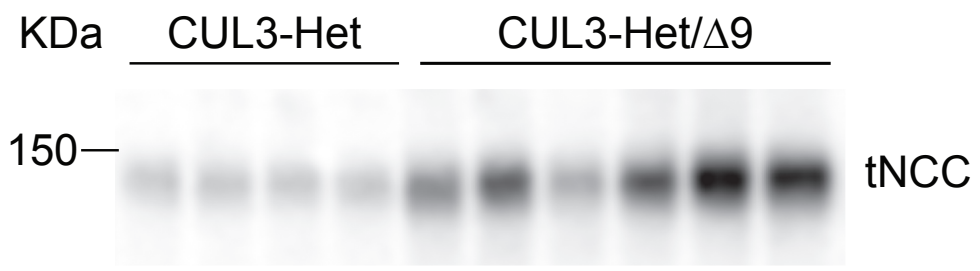

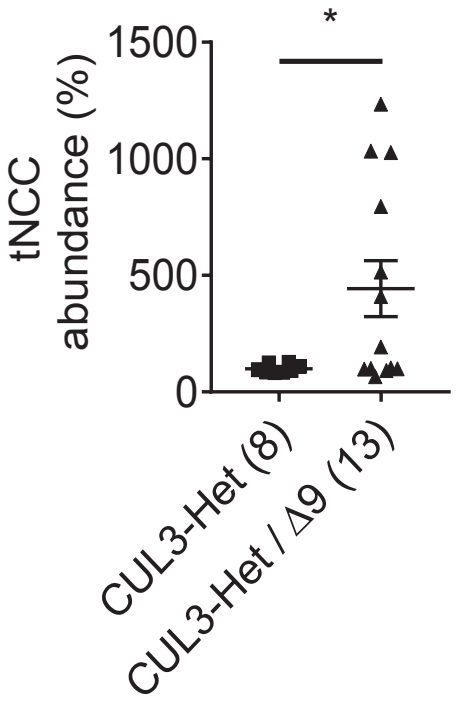

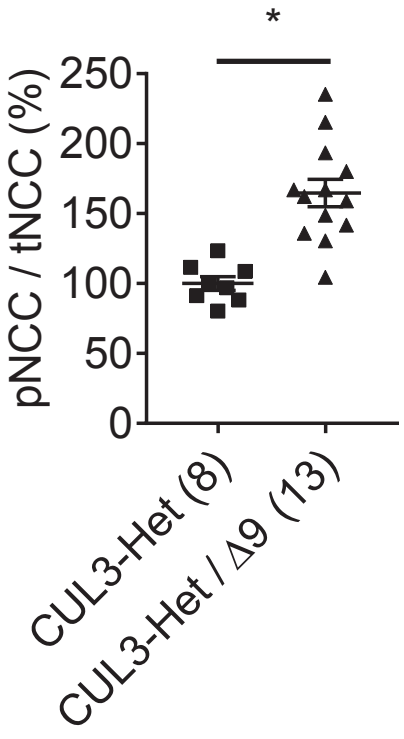

Supplementary Figure 5.

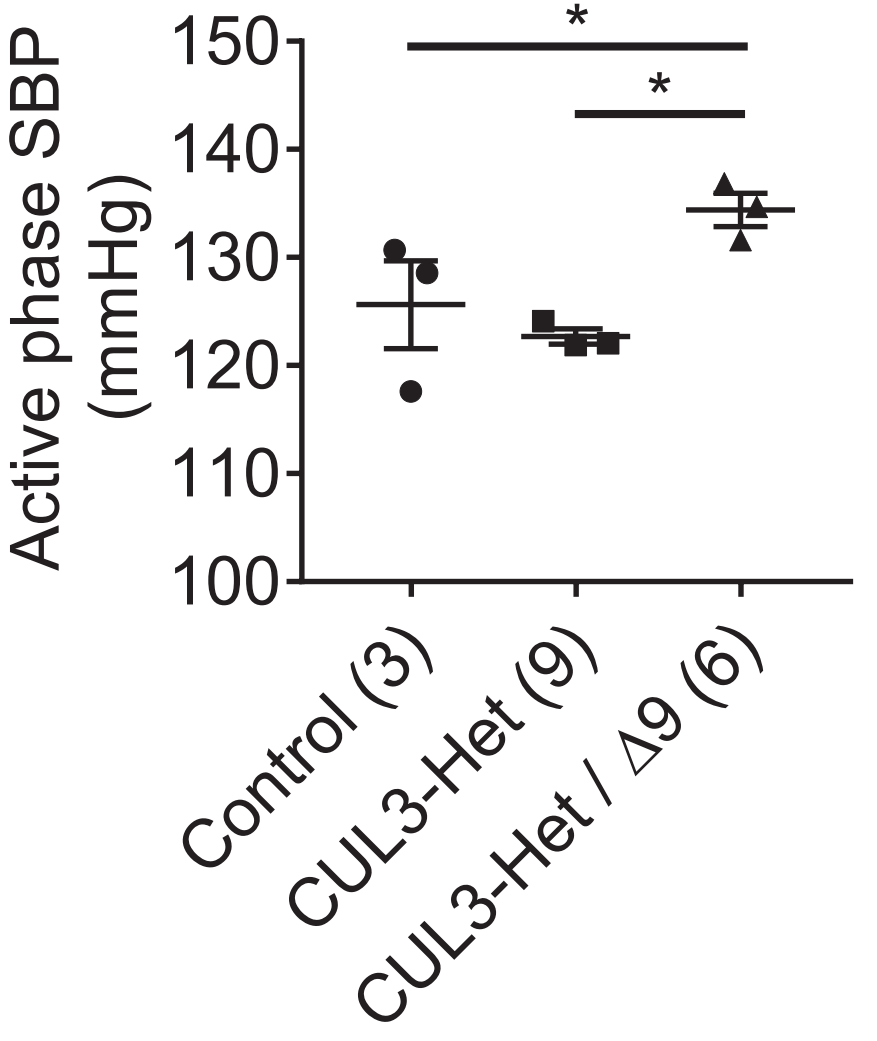

Supplementary Figure 6.

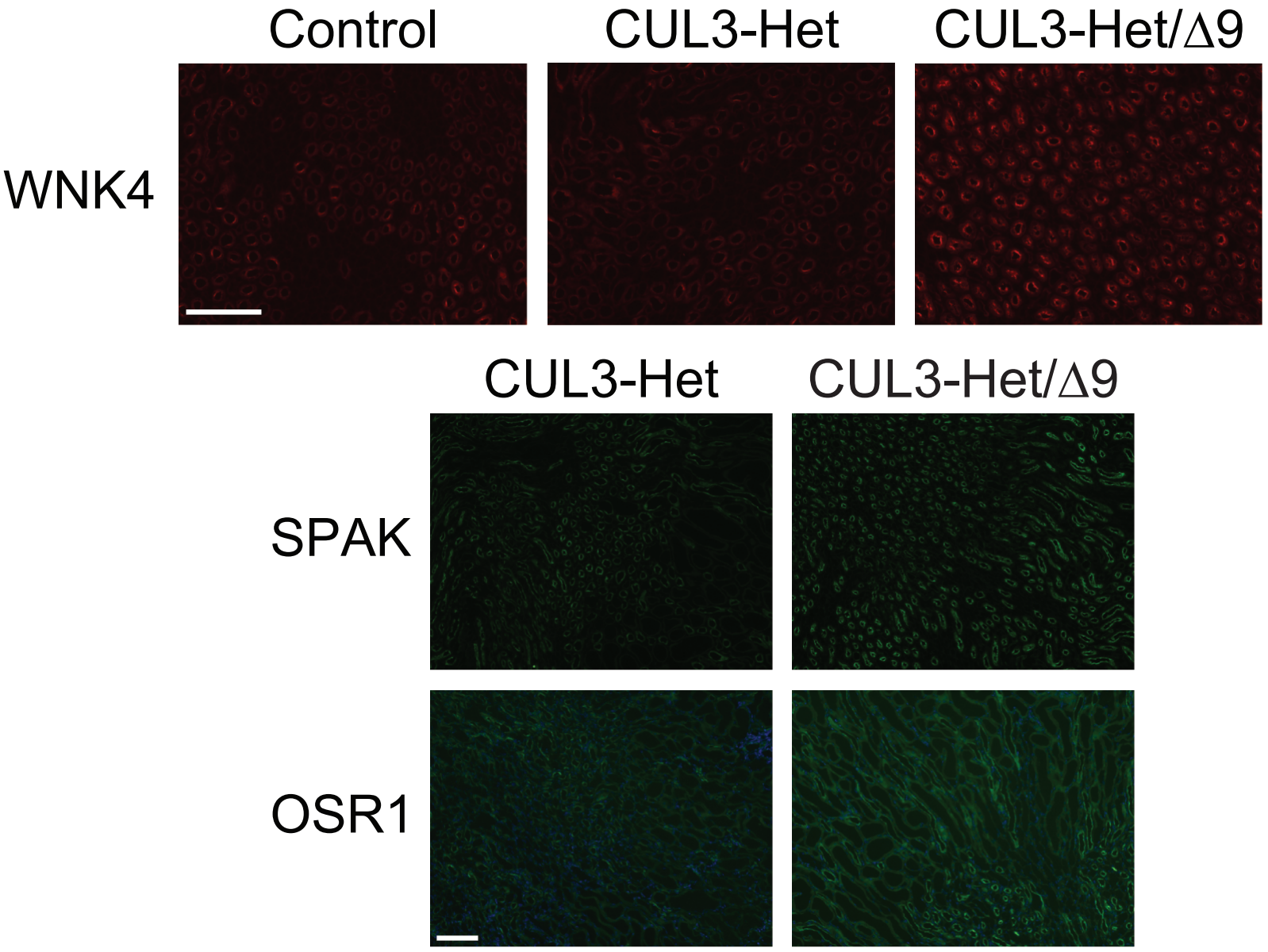

Supplementary Figure 7.

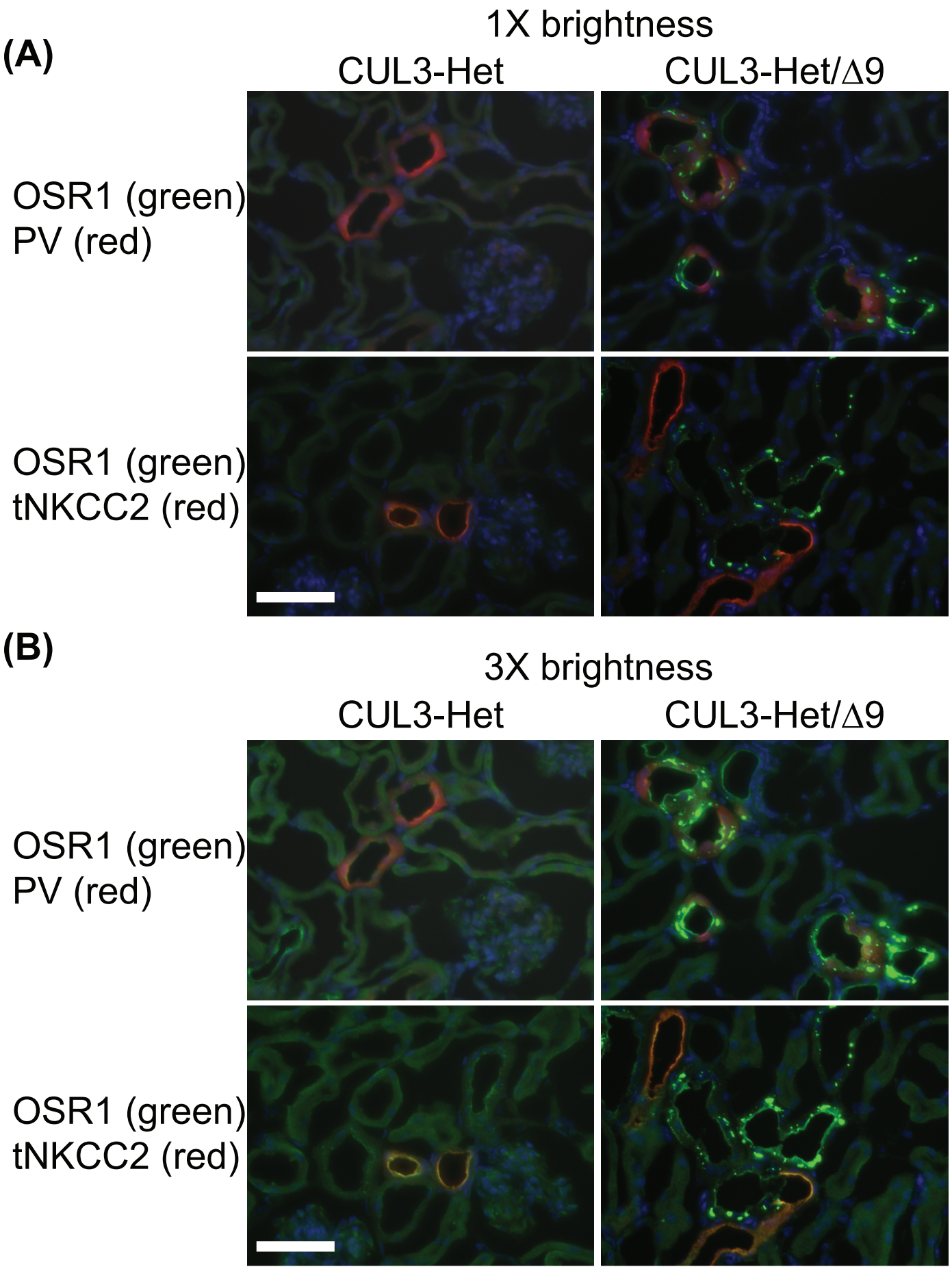

Supplementary Figure 8.

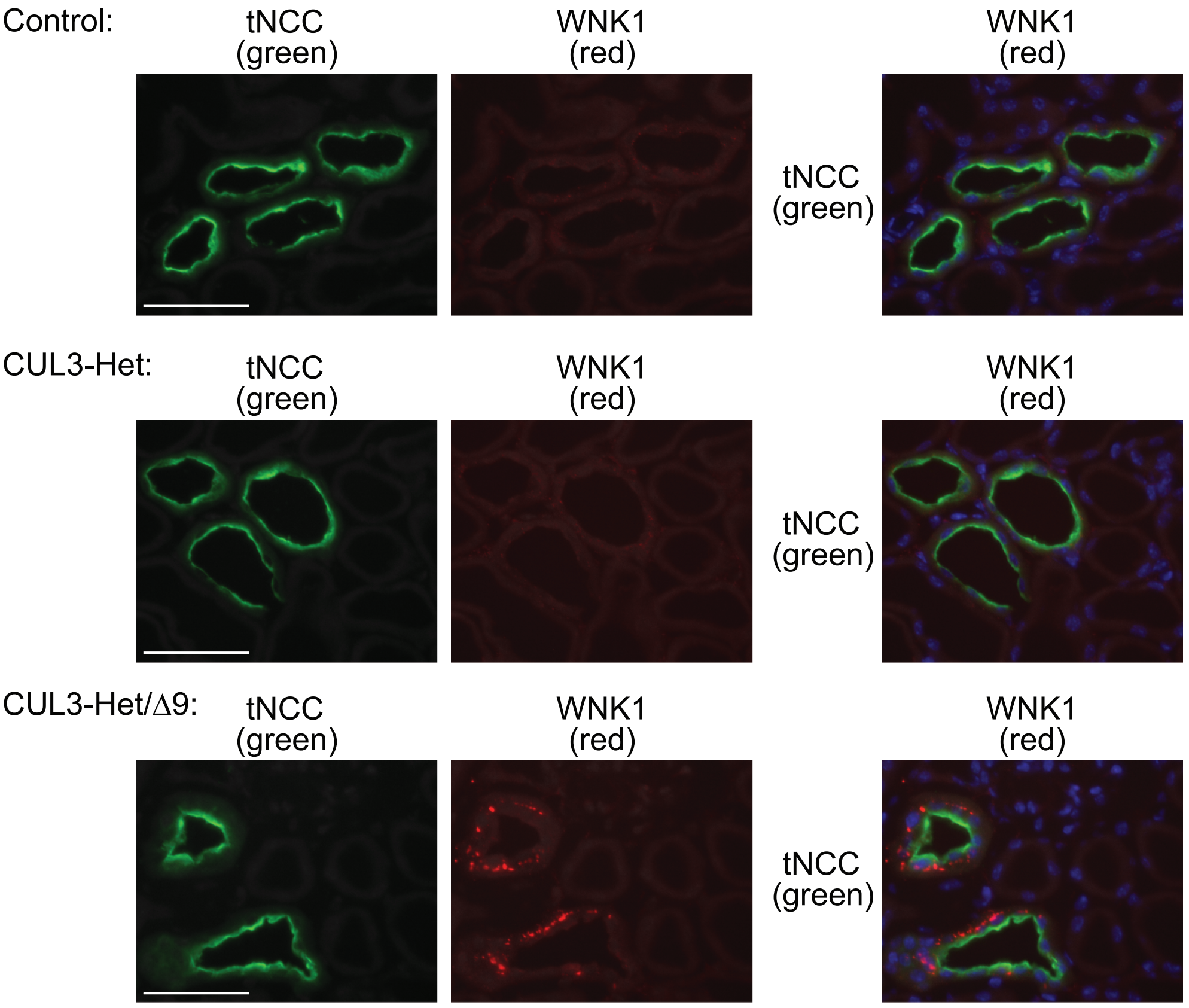

Supplementary Figure 9.

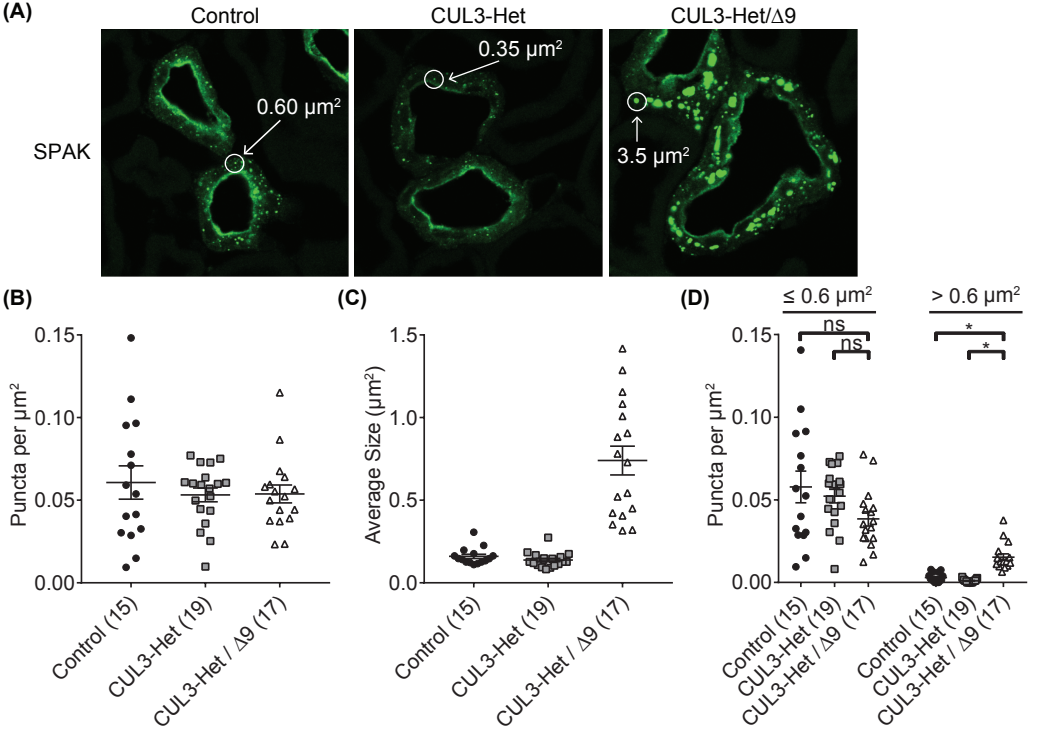

Supplementary Figure 10.

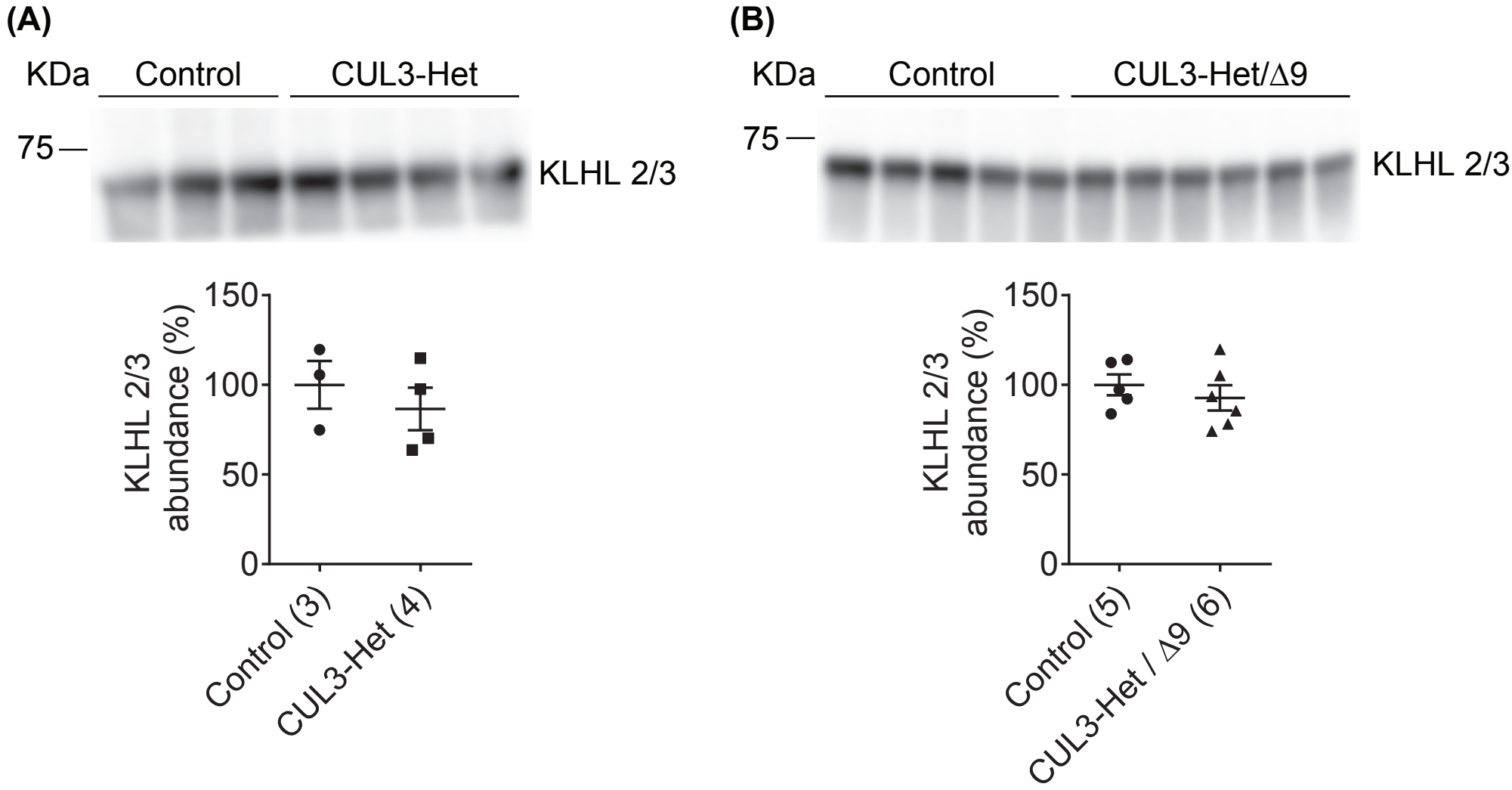

Supplementary Figure 11.